Journal of
Ceramic Science
and Technology

J. Ceram. Sci. Technol., **08** [2] 277-286 (2017)
DOI: 10.4416/JCST2017-00009
available online at: http://www.ceramic-science.com

Influence of Material and Processing Parameters on the Surface Roughness of Injection-Molded Ceramic Parts

S. Greiner*[1], K. Kurth[1], C. Fix, T. Braun[2], J. Franke[2], D. Drummer[1]

[1]Institute of Polymer Technology, Friedrich-Alexander-University (FAU) Erlangen-Nürnberg
[2]Institute for Factory Automation and Production Systems, Friedrich-Alexander-University (FAU) Erlangen-Nürnberg

received Febuary 9, 2017; received in revised form Febuary 17, 2017; accepted March 16, 2017

Abstract

Ceramic parts were prepared by means of injection molding and a two-step debinding and sintering process. For four different alumina ceramic feedstocks, the influence of processing parameters like holding pressure, injection speed, melt and mold temperature on the surface roughness was studied. The surface roughness was measured in the direction of flow and perpendicular to it with a tactile cantilever measuring system. A gradient in the surface roughness is detected along the flow path, which ended in a relatively coarse surface section. Smoother and more even surface structures can be generated with higher mold temperatures. In general, larger particle diameters cause greater surface roughness. Lower injection speed and melt temperature show similar effects. However, no significant effect was observed with regard to the holding pressure. Based on these results, the surface roughness could be adjusted in a certain range by changing material or processing parameters in order to fulfill the requirements of a subsequent metallization step.

Keywords: Ceramic injection molding, surface roughness, ceramic feedstock, Al_2O_3 ceramics

I. Introduction

Ceramic injection molding allows the fabrication of small parts with reproducible, highly complex and near-net-shape structures in large quantities [1,2]. The process is divided into four steps. First, a ceramic powder, such as alumina, is mixed with a binder and compounded to prepare the ceramic feedstock. The binder typically consists of at least two polymeric phases, plasticizers, lubricant components and additives such as surfactants [2]. The feedstock can be injection-molded to form green compacts in regular polymer injection molding machines, which are resistant to abrasive materials. Afterwards the binder has to be removed from the fabricated parts, which is often achieved with a combination of solvent and thermal debinding. Since debinding can generally be seen as the most critical process step, much effort has to be channeled into optimum debinding strategies and kinetics [3,10]. Finally, the porous brown part is sintered and densified to a compact ceramic part [1].

Oxide ceramics are electrically insulating, withstand high temperatures and are chemically resistant to most solvents and extremely resistant to wear [11]. For most technical and medical applications, smooth surfaces with low surface roughness are desired in order to highlight the ceramics' favorable wear properties. Nevertheless, thanks to this spectrum of properties, their use has recently been emphasized as substrate material for three-dimensional circuit carriers of high-temperature-resistant sensors in 3D-Molded Interconnect Device (3D-MID) technology [12,13].

Miniaturizing of electronic devices in combination with high voltages and currents leads to high punctual thermal stresses, for which most of the polymers such as standard and technical thermoplasts are not suitable. Compared to these polymers, ceramics are resistant to high temperatures, exhibit low thermal expansion and sustain chemically challenging environments [11]. For this reason, functionalized ceramics have been proposed as substrate materials for electronic devices in fields like the general electronics, aerospace, nuclear power and the automotive industries [14,15]. To date, one of the greatest challenges to metallizing ceramics is the poor adhesion between the metal and ceramic surfaces, which generally complicates the application of a highly adhesive metal layer onto a ceramic substrate [14]. The differing chemical constitution of metals and ceramics in addition to their wide-ranging differences in material properties, such as wettability [16] and thermal expansion [17], are crucial for high-temperature coating processes. It has been pointed out that the adhesion of conductor tracks can be adjusted by enhancing the chemical reactivity between the components [17–19] and by optimizing the material interface. Furthermore, for the fabrication of a strongly adhesive metal layer, the ceramic surface should feature a uniformly high surface roughness [20] and at best have undercuts for mechanical linkage [21]. Compared to filled polymers, the production of ceramic parts with mi-

* Corresponding author: greiner@lkt.uni-erlangen.de

cro-structured undercuts is problematic because of the final sintering and densifying process, which leads to the reduction of these desired structures.

However, we think that enhanced surface roughness could improve the physical adhesion of the metallized layers [20] and that this can be influenced by the injection molding process [22, 23]. Islam *et al.* [24] investigated the shrinkage and the surface replication of Y_2O_3-stabilized ZrO_2 parts with different mold surfaces. They showed that rough surfaces could be replicated well with injection molding and sintering. A smoothening effect of the sintering process on the surface could be proven as well as different roughnesses along the flow path from close to the gate to far from the gate [24].

Zhang *et al.* [22] stated that surface roughness can be optimized not only with the mold surface but also with the powder grain size, the debinding process, sintering parameters and other influencing factors, but provided no clear evidence of the influence of injection pressure, mold temperature or holding temperature on the surface roughness of ceramic green microstructures [22]. To date, typical approaches to increase the surface roughness include chemical etching [18] and shot peening [14].

In this work, the surface roughness of injection-molded alumina parts has been studied along the flow path and according to the flow direction, as ceramics with adjusted surface roughness may be desirable for subsequent functionalization such as metallization. The aim of this work is to determine parameters that could allow the fabrication of rough-surface ceramic components by means of injection molding so that sintered alumina substrates could be metallized directly and without pretreatment. Accordingly, the influence of processing parameters, such as mold temperature, melt temperature, holding pressure and injection speed on the surface structure is evaluated in order to identify parameters for enhancing surface roughness.

II. Experimental

In these investigations, commercially available aluminum oxide feedstocks Inmafeed K1008, Inmafeed K1010 and Inmafeed K1013 (Inmatec Technologies GmbH) were used. In addition, a feedstock was prepared in a dual-screw extruder (Leistritz ZSE HP 27). Therefore, 15 wt% inorganic binder, consisting of two binders Embemould K83 and Embemould K83G (eMBe Products & Service GmbH) in a 1:1 ratio, was compounded with 85 wt% alumina powder CT3000SG (Almatis GmbH). This is equivalent to a filler content of approximately 60 vol%. The particle size distribution of the CT3000SG alumina powders was obtained with an optical measuring system (Morphologi G3, Malvern) analyzing 100 000 particles, which is equivalent to 0.7 mg weight of the sample taken. The measured values are compared to manufacturer specifications. The particle form of highly filled polymers can influence orientations in the edge layers and along the melt front, and for this reason cause anisotropic mechanical behavior. Hence, the particle morphology of the CT3000SG powder was investigated by means of scanning electron microscopy (SEM) at 10 000x magnification with an excitation voltage of 5 kV (Ultra Plus, Carl Zeiss AG).

The filler content of all ceramic feedstocks was measured with thermogravimetric analysis (TGA; Q 5000, TA-Instruments). Owing to high possible material property variations of the granulated feedstock, the thermal material behavior was examined with differential scanning calorimetry (DSC) and a sample size of three with a heating rate of 10 K/min (Q2000, Texas Instruments). The mean value graphs of the second heating will be shown and discussed. The melt volume rate was determined for all feedstocks in accordance with DIN EN ISO 1133 for a temperature of 150 °C and a loading mass of 21.6 kg. Preheating time was 300 s and the cut-off length was set to 3 mm.

Rectangular green test specimens measuring 70 x 45 x 2.5 mm^3 were prepared by means of the ceramic injection molding of the four feedstocks on a two-component injection molding machine Engel ES 220H/200V/80HL (Engel Deutschland GmbH). The horizontal injection unit with a ceramic screw measuring 25 mm in diameter was applied. The injection molding machine had a maximum clamping force of 900 kN. The processing parameters are given in Table 1, the parameter set P1 being defined as the reference parameter set. In the following experiments, the holding pressure, melt and mold temperature and the injection speed were varied and compared to the reference. The cooling time was set to 25 s.

For testing the mechanical properties induced by the processing set-up, 4-point bending tests were performed on the green compacts in compliance with DIN EN 843 – 1. The testing speed was set to 0.5 mm/min for the ten bending samples for each parameter set. In order to characterize possible feedstock demixing, thermogravimetric analyses were performed on green compacts of K1010 and CT3000SG. For this reason, samples of approximately 30 mg were taken from three sites along the flow path and then incinerated (TGA Q 5000, TA-Instruments). The number of samples taken was three.

Table 1: Processing parameters for ceramic injection molded green parts.

Parameter Set	Unit	P1	P2	P3	P4	P5
Melt temperature	°C	140 – 160	140 – 160	140 – 160	140 – 160	**159 – 161**
Mold temperature	°C	55	55	**65**	55	55
Holding pressure	bar	300	**0**	300	300	300
Holding time	s	5	**0**	5	5	5
Injection speed	mm/s	20	20	20	**10**	20

The water-soluble content of the green compacts was removed in deionized water for 80 h and the green compacts were subsequently freed from backbone polymer by means of thermal debinding at maximum temperatures of 300 °C for approximately 42 h. The porous brown parts were cooled down and subsequently sintered for approximately 22 h following a defined program with a maximum temperature of 1680 °C and afterwards cooled down to room temperature. The surface roughness of the molded green parts and sintered ceramic components was determined in accordance with the standard DIN EN 623 – 4:2004 using the contact profile method (Hommel Tester T1000, Osterwalder AG). In the experiments a 5-µm hard-metal probe tip with 90° opening angle (Jenoptik Industrial Metrology Germany GmbH) was employed. As shown in Fig. 1, the samples' surface was divided into four sections along the flow path. In order to evaluate the influence of the flow behavior, the surface roughness was measured in the direction of flow and perpendicular to it. In these investigations, the mean roughness depth R_z of the specimens was interpreted. According to the standard, the measuring section was 4.8 mm including 0.8 mm cut-off. For calculating the mean roughness depth, the measuring section is divided into five sampling lengths, which are averaged. Within these sections, the distance from the highest peak to the lowest valley is measured. The vertical measuring range was 80 µm. The sample size n for each measuring location was five.

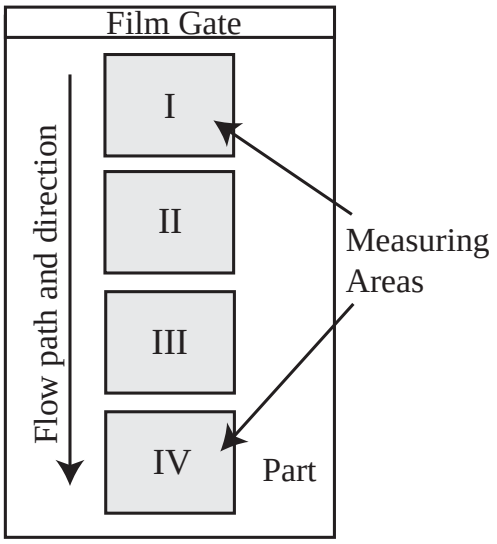

Fig. 1: Schematic showing the areas for the surface roughness measurements.

To characterize the topology of the ceramic parts, SEM analyses were conducted with 1000 × magnification and shown for the K1010 and CT3000SG feedstocks (Ultra Plus, Carl Zeiss AG). In addition, a 1000 ×-magnified SEM cross-section of an already metallized ceramic is shown to demonstrate the potential of mechanical linking of a rough ceramic substrate.

III. Results and Discussion

(1) Material and feedstock characterization

The values of the measured diameters of the numerical particle size distribution are shown in Table 2. The manufacturer specifications indicate that the mean particle diameter of all materials varies in a relatively narrow range from 0.4 to 2.1 µm, K1013 having the smallest mean particle size and K1008 the largest. For the coarsest material, 90 % of the particles have a grain size smaller than 6.2 µm, which indicates a very narrow range of particle sizes from 0.1 to under 10 µm for all systems examined. In a comparison of the results of the CT3000SG measurements with the specifications, marginally higher values were measured, which can be assigned to the different measuring systems and dispersing units. Nevertheless, both measurements show a mean particle diameter of below one micrometer and a D90 of less than 3 µm.

A SEM image of the CT3000SG powder is shown in Fig. 2. SEM images of powders obtained by means of the incineration of K1008, K1010 and K1013 feedstocks can be found in [25]. The image shows relatively homogeneous and fine-sized particles of the sample analyzed. In the close-up view, the coarse and angular form of the platelet particles can be observed. On the one hand, this edgy form could endow the green compacts with higher strength, but on the other hand reduce the flowability of the ceramic feedstock [1]. This effect could even be intensified by the small particle sizes, as most of the Al_2O_3-particles are sized below 1 µm in diameter. With regard to the observed particle diameters, this result is in accordance with the measurements of the particle size distribution. Nevertheless, small particle sizes offer a large specific surface that enhances the material's sintering activity and reduces the chance of molding defects [1]. This can lead to better mechanical properties of the green part and a higher component strength of the final ceramic part. However, if the content of the binder is not varied, a decrease in particle size leads to higher feedstock viscosity.

With the selected testing conditions, values for the melt volume rate (MVR) could only be generated for the K1008 and K1010 feedstocks, the results are shown in Table 3. At a constant pressure level, the other materials did not show sufficient flow behavior for these measurements, including temperature variations from 140 to 160 °C. This can be explained by the lack of shearing, as the feedstocks have shown sufficient flow behavior during injection molding. Nevertheless, it can be seen that despite the high standard deviation, K1010 has a much higher melt volume rate of 26 cm^3/10 min compared to the MVR of K1008, which is around 7 cm^3/10 min. This means that K1010 probably has the lowest viscosity of all examined feedstocks, which could be attributed to a homogeneous particle distribution, spherical particles or an optimized and an excellently flowing binder system. These results could indicate better processibility of K1010 than of any of the other feedstocks, whereas other materials might be more abrasive on the injection molding unit, leading to increased contamination, which could cause imperfections after sintering and in turn result in reduced breaking resistance.

Table 2: Particle size distribution of alumina particles in selected feedstocks.

Diameter	Unit	CT3000SG	CT3000SG*	K1008*	K1010*	K1013*
D_{10}	µm	0.4	0.1	0.1	0.5	-
D_{50}	µm	0.9	0.5	2.1	1.2	0.4
D_{90}	µm	1.7	2.6	6.2	2.7	-

* manufacturer specifications

Table 3: Melt volume rate at 150 °C and filler content measured by thermogravimetric analysis of studied ceramic feedstocks.

	Unit	CT3000SG	K1008 KMS-96 BO	K1010 CT1200SG	K1013 AES-11C
MVR	cm³/10 min	not flowable	7.3 ± 0.1	26.4 ± 3.7	not flowable
TGA	wt%	84.5	84.5	85.3	84.1

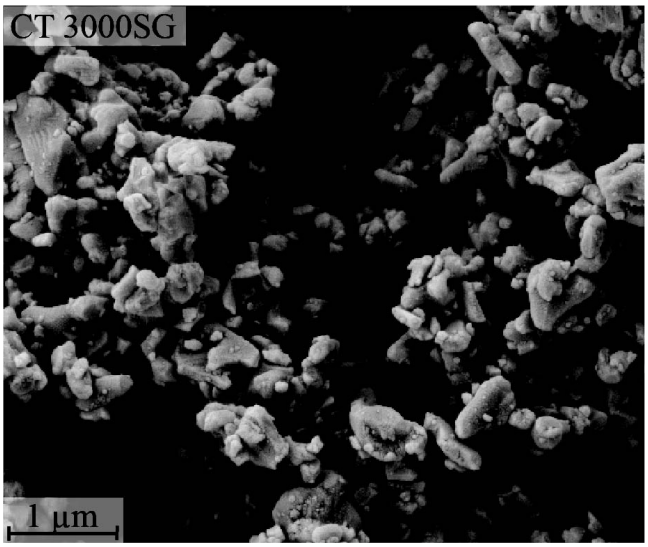

Fig. 2: Scanning electron microscopy images of Al_2O_3 (CT3000SG) powder particles at 10000 × magnification.

The filler contents of the commercial feedstocks is proven by means of thermogravimetric analysis and determined for the compounded feedstock containing CT3000SG. The aim was to produce a feedstock with a filler content comparable to commercial products. The exact values are given in Table 3. Preliminary studies have shown that the binder used burns out completely in oxygen atmosphere so that no signal noise from burnt polymer can be expected. The weight of all specimens decreases slightly to around 98 wt%, but almost linearly until 350 °C. At even higher temperatures thermal decomposition of the binder is initiated and continues linearly up to around 500 °C. The specimen's mass remains stable at a percentage of around 85 wt%, which is the remaining filler content of the commercial products and the targeted value of the compounded feedstock. These results indicate similar filler contents for the examined feedstocks, which is relevant for the comparability of downstream analyses, e.g. sintering shrinkage or porosity.

In Fig. 3, the results of the DSC analysis for second heating of the ceramic feedstocks are shown. The exact values for the different melting points from TM1 to TM3 and the melting enthalpy HM1 are given for the different ceramic feedstocks in Table 4. In a comparison of the measured heat flow curves, quite similar runs can be observed. In these curves, one main melting peak can be observed at around 60 °C, which refers to the low-viscosity wax and probably water-soluble component of the binder.

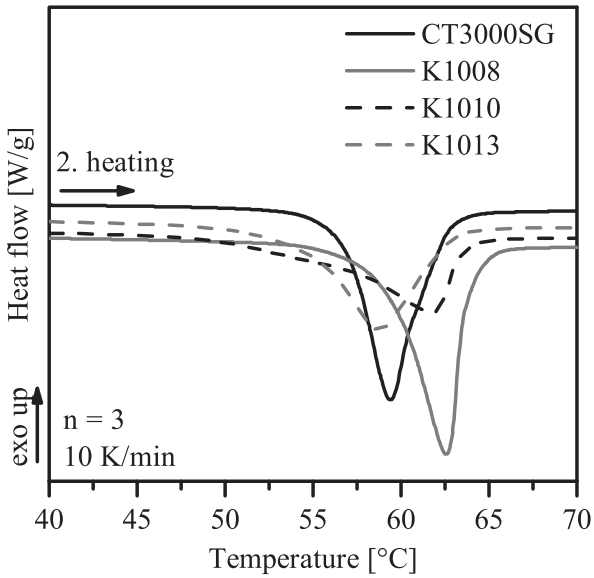

Fig. 3: DSC analysis of the ceramic feedstocks at the second heating.

Nonetheless, two more slight slopes can be observed at around 110 and 160 °C, which can be associated with the so-called backbone polymers and are present at lower concentrations compared to the wax component. As the exact compositions of the binders are not known, the influence of additives like stabilizators and lubricants on the thermal behavior of the binder cannot be determined. However, the main melting points in Fig. 3 show that the exact composition of the four feedstocks are different. Similar polymers from different manufacturers or differing additives may have been applied. Nevertheless, this result shows that based on the polymeric components, processing with the same parameter set seems possible, disregarding particle size, form and particle size distribution of the alumina which influences the viscosity of the composite material.

Table 4: Melting temperatures and melting enthalpy extracted from DSC analysis of different ceramic feedstocks.

	Unit	CT3000SG	K1008 KMS-96 BO	K1010 CT1200SG	K1013 AES-11C
T_{M1}	°C	59.4	62.4	61.6	59.0
T_{M2}	°C	111.5	111.5	108.3	109.5
T_{M3}	°C	157.5	158.9	159.5	157.7
H_{M1}	J/g	12.0	12.7	9.7	10.6

(2) Mechanical characterization of green bodies

The results of the 4-point bending test of the injection-molded green parts are shown in Fig. 4. The flexural strength is presented for the different parameter sets and ceramic feedstocks. For all measurements, the values for the maximum tension vary between 12 and 22 N/mm². An influence of different parameter variations on the maximum stress can hardly be distinguished, but the results for the material variations vary in a significant way. The highest values of 18 to 22 N/mm² are achieved by the commercial K1010 and K1008 feedstocks, probably owing to appropriate particle size distribution and optimized binder system. K1013 lies slightly below these values, possibly owing to its small particle size, which could have led to particle agglomeration, so that not all particles are wetted homogeneously. The lowest values overall were measured for the compounded feedstocks. Reasons for this might be different pretreatments of powder or binder and lower material purity, which could lead to the earlier failure of the bending specimens owing to reduced adhesion between binder and ceramic particles. Nonetheless, for the parameter sets P2, P3 and P5, the values are quite close to those of the commercial products.

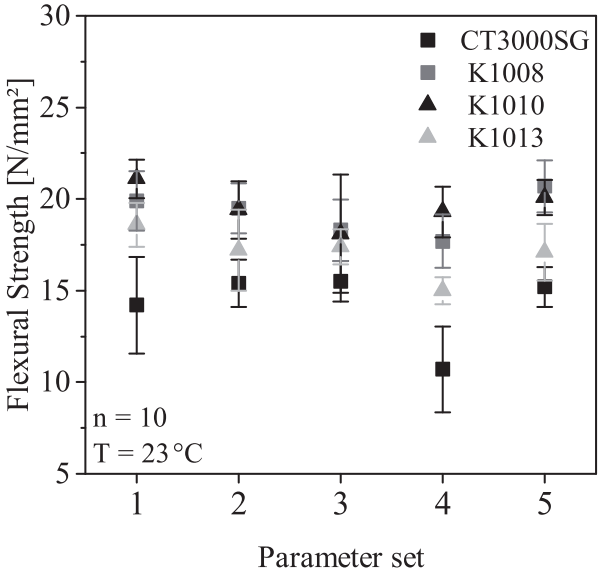

Fig. 4: Flexural strength of injection-molded green parts determined in a 4-point bending test.

(3) Characterization of the surface roughness

The following section will give a detailed overview of the surface roughness of injection-molded ceramic feedstocks. The aim of this research was to modify and to enhance or rather increase the surface roughness of injection-molded ceramics to establish a good starting situation for subsequent metallization. In general, different assumptions have to be taken into account, because of the two counteracting processes caused by the two subsequent processing steps, debinding and sintering. On the one hand, binder removal leads to a porous part with a relatively rough surface, while on the other hand the thermal influence during solid-state sintering establishes a minimized surface, which means that sharp edges and pores are avoided by surface diffusion. A smooth and slightly wavy surface would be the result. In ceramic injection molding, geometric details have to be realized during the injection molding process as ceramic post-processing is very expensive and time-consuming. This is mainly valid for geometric aspects but has to be proven for superficial features such as surface roughness. In the following diagrams, the feedstocks are sorted according to the mean particle diameter D50 of the applied ceramic powders.

For this reason, green compacts and sintered parts were analyzed in order to characterize the transferability of the surface structure from green part to the final part. Sufficient transferability is necessary to allow surface manipulation in the injection molding process. In Fig. 5, the results for the measurements in the direction of flow and perpendicular to it are shown for the four different feedstocks and their green and sintered parts. Within the standard parameter set P1, green parts reach mean surface roughnesses of approximately 4 µm, but are subject to relatively high measurement uncertainties. For the CT3000SG feedstock, the roughness of the sintered part is almost equal to that of the initial green body. Only for K1013 does the green body have a higher roughness. K1010 and K1008 sintered parts show the highest roughnesses.

Taking a closer look at the particle diameters again, it can be seen that K1013 has the smallest mean particle diameter, followed by CT3000SG, K1010 and K1008, which leads to assumption that the transferability of green body roughness is related to the powders' mean diameter or the particle size distribution. In this case, the phenomenon could be described by the powder packing density at the surface. It is well known that smaller particles can lead to smoother surfaces. In addition, this effect is emphasized by the increased sintering activity of smaller particles owing to their larger specific surface area. After reaching a certain limit, the effect of surface smoothening during sintering seems to be higher than the surface roughening effect caused by binder removal, such that the green body has greater surface roughness than the sintered part. This effect can fur-

ther be proven by the results of the measurements perpendicular to the flow direction, which are also shown in Fig. 5.

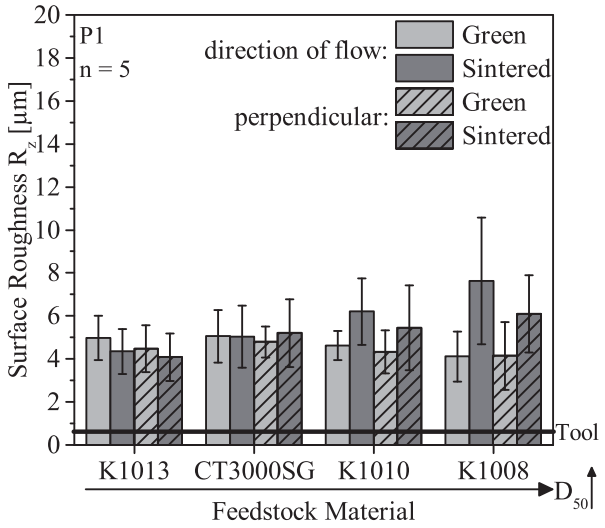

Fig. 5: Comparison of the surface roughness of green parts and sintered parts prepared from different feedstocks measured in direction of flow and perpendicular to it.

The mean values are almost comparable to those of the measurements in the direction of flow. Therefore, it can be stated that possible orientations have no significant influence on the surface roughness for the standard parameter set. For that reason, the following results are shown predominantly for measurements in the direction of flow.

In Fig. 6 and Fig. 8, the measured values for the surface roughness of different materials are shown along the flow path for the standard parameter set P1 and for the parameter set P5. The area of the specimen is divided into four sections along the flow path, which is 70 mm for green parts and, because of shrinkage, approximately 60 mm after sintering. Section I is close to the gate and IV is the furthermost measuring area. In Fig. 6, different results can be observed. Specimens of CT3000SG seem to have a quite similar surface roughness from section I to III, only section IV seems to be an exception. For K1013, the same effect at lesser roughness can be seen. The typical demixing process for highly filled polymers leads to lower filler contents at the end of the flow path, which is in accordance with higher porosity after debinding. For CT3000SG, the results of the thermogravimetric analysis indicate a slight feedstock demixing of around 1 wt% from the gate (section I) to the end of the flow path (section IV). This could explain the greater roughness of sintered parts at section VI. In addition, an insufficient filling of the mold cavity caused by the relatively long flow path could be causal to that phenomenon. For K1010, the filler content remained stable along the flow path. For this reason, this effect cannot be observed for K1010 specimens, which seem to have a more homogeneously distributed surface roughness, despite higher standard deviations. For K1010, no significant relationship between surface roughness and flow path can be derived preliminarily.

The SEM images in Fig. 7 show the topological difference of the part surface between the compounded CT3000SG and the K1010 feedstock. For both materials, fine fissures are visible close to the gate, which can be attributed to the cavity filling. For CT3000SG the surface becomes even rougher, whereas the structure of K1010 remains stable. This can be explained by the lower viscosity of the material. When the material is compressed at the end of the flow path, the viscosity of K1010 is low enough to generate a homogeneous layer and surface, whereas for CT1200SG the flow fronts are not able to fuse together.

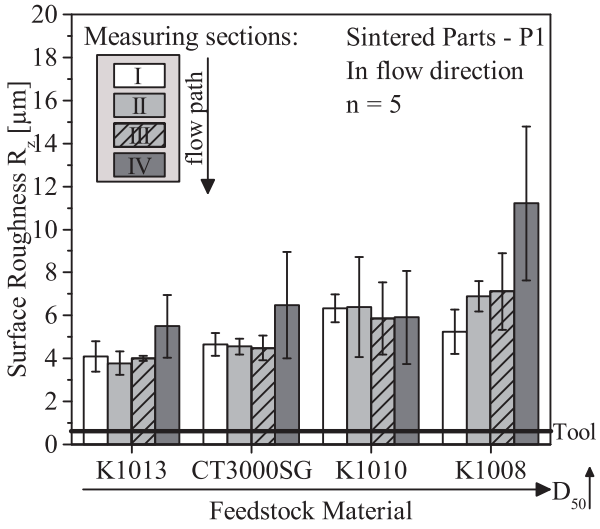

Fig. 6: Characterization of the surface roughness of sintered ceramic parts along the flow path in flow direction for the standard parameter set.

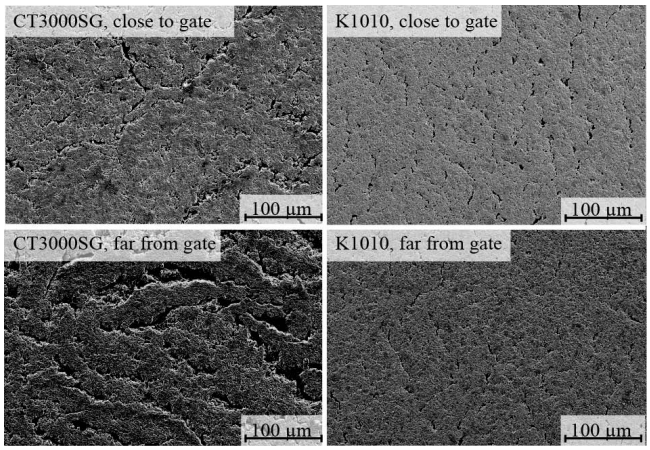

Fig. 7: SEM images of K1010 with a low gradient in surface roughness and high gradient along the flow path for CT3000SG.

In Fig. 8, the surface measurements for the different feedstocks of sintered parts produced with parameter set-up P5 are shown. In this overview, greater differences in terms of surface roughness can be seen at the end of the flow path. In fact, for K1013 and CT3000SG the values are almost doubled with an increase of more than 4 µm. Again, this result has to be associated to the demixing behavior of the components' different densities or insufficient filling of the mold cavity and is further intensified by a higher melt temperature. After debinding, the area at the end of the flow path is even more porous, leading again to enhanced roughness. For metallization, pronounced surface roughness is desired, but nonetheless the surface roughness has to be homogeneously distributed rather than a

show a graded behavior. In the comparison of the absolute surface roughnesses of materials processed with different parameter settings, in the following, section IV will be omitted as the focus is on uniform surface roughness.

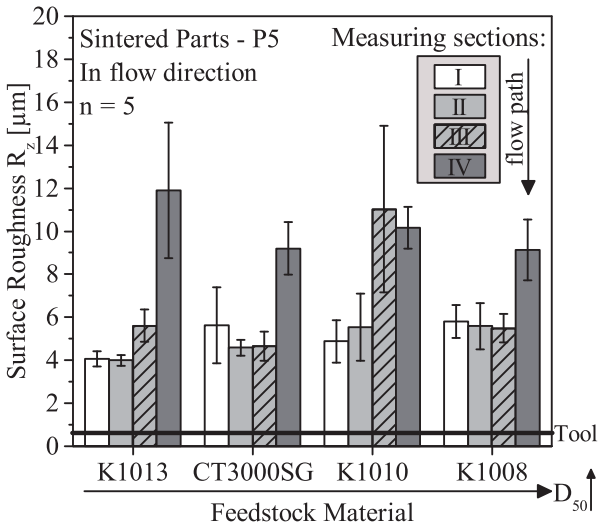

Fig. 8: Characterization of the surface roughness of sintered ceramic parts along the flow path in flow direction for parameter set P5.

The results of the parameter studies of sintered ceramic parts measured in direction of flow are shown in Fig. 9. The calculated mean values range between 2 and 9 µm and are not exclusively dependent on the particle diameter of the ceramic powder but also on the processing parameters. For all materials, an almost similar profile regarding the values for the different parameter sets can be observed, which indicates that a manipulation of the surface roughness of ceramic parts by variation of the injection molding processing parameters is generally possible. The results of the standard parameter set P1 indicate increasing surface roughness with increasing mean particle diameter, which can be seen as the ceramic feedstocks are sorted according to mean particle size in the diagram. Leaving out holding pressure, as shown for the measurements in parameter set P2, has almost no influence on the generation of the surface structure. For this result, several explanations can be considered. The applied force of this holding pressure might either have been too low or the sealing time might already have been reached. As the applied materials are highly filled systems and only around 40 vol% consists of a compressible polymeric component, it is more likely that the holding pressure can hardly press in any further material, which could have led to a varied situation concerning the development of a surface structure.

However, higher mold temperature typically improves the flow behavior of polymeric melts and the replication of the mold surface. As shown for parameter set P3, the surface becomes smoother with reduced surface roughness. Higher mold temperature leads to slower cooling of the edge layers, which leads to better flowability and filling of the cavity. In addition, this could reduce a possible occurrence of feedstock demixing, leading to a smoother surface. In parameter set P4, the injection speed is reduced, which leads to longer injection time and greater surface roughness for K1013 and CT3000SG, whereas the roughness for K1010 is almost unchanged and for K1008 this leads to reduced roughness.

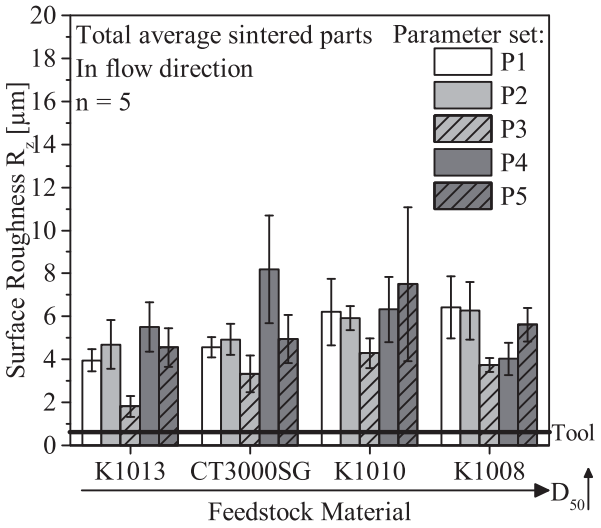

Fig. 9: Influence of material and processing parameters on the surface of sintered parts measured in direction of flow.

Again, a relationship between the effect and the mean particle size can be taken into account. With small particle diameters, the roughness is increased. This could be explained by an orientation of the platelet particles perpendicular to the movement of the melt. It is possible that with increasing particle diameter, the particles tend to hinder one another in their rotatory orientation movement. Higher melt temperature as shown for P5 leads to slightly increased roughness for K1013, CT3000SG and for K1010 feedstocks but for to decreased values K1008. According to the data sheet, the binder of the feedstock begins to degrade at 160 °C, which could eventually lead to alternating surface morphology, but also the viscosity drop could have changed the flowing behavior. It could be shown that with the use of different processing parameters and minor material parameter changes, the surface roughness can be changed slightly, in a range of approximately 10 µm. In addition, the surface of green parts allows first estimations of the surface roughness of the final sintered ceramic parts.

In Fig. 10, the cross-section of an alumina plate metallized by means of plasma-coating technology is shown. A relatively homogeneous surface roughness can be observed close to the gate. The deposited copper layer is capable of filling the voids. Far from the gate, greater surface roughness can be observed, which can lead to improved layer adhesion. According to this result, better adhesion can be expected with enhanced surface roughness, which leads to better linking of the two components.

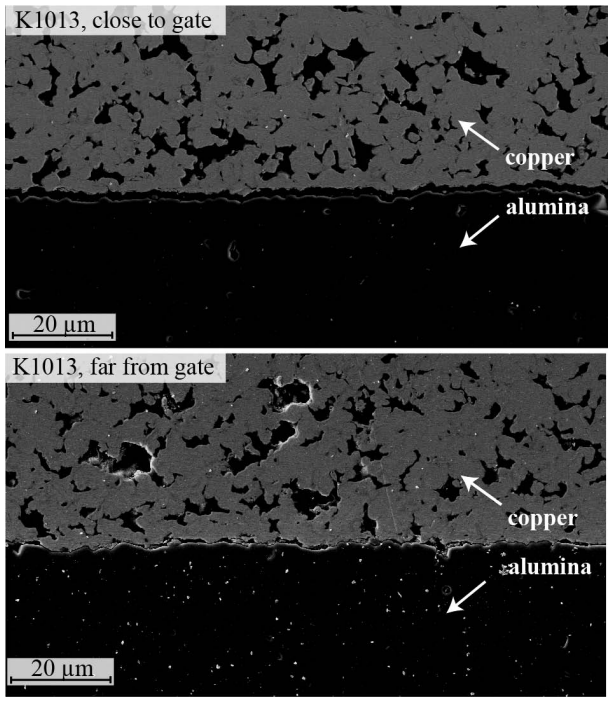

Fig. 10: SEM images of an alumina substrate metallized with cold-active plasma.

IV. Conclusions and Outlook

In this work, first the properties of the materials studied were characterized in order to determine the influence of material and processing parameters on their mechanical bending strength and surface roughness. A certain degree of surface roughness is required to achieve sufficient adhesive strength of a metallic layer applied, for example, with plasma-coating technology. It could be shown that maximum stress is mainly material- or rather feedstock-dependent, but can be improved by changing the processing parameters. In terms of surface roughness, the material properties, such as the mean particle size diameter, play a crucial role. If pronounced surface roughness is desired, large particle sizes should be chosen. Not only the measured roughness itself is important, the shape of the surface such as homogeneous distribution of elevations and valleys must be taken into consideration. Substantial differences, which are caused by demixing along the flow paths and eventually insufficient filling of the cavity, have to be taken into account and avoided when homogeneously rough surfaces are required. According to these results, the surface finish of injection-molded feedstocks could be varied slightly depending on the processing parameters applied. Especially increasing or decreasing mold temperature or injection speed could lead to changed surface structures in a certain range. In follow-up studies, the influence of the mold design on the surface roughness of different feedstocks and injection-molded ceramic parts will be investigated. Therefore, molds with differently eroded structures will be set up and their moldability using ceramic feedstocks will be studied.

Acknowledgments

The IGF Project 18551 N CIMAMET of the research association "Räumliche Elektronische Baugruppen 3-D MID e.V". was, on the basis of a resolution of the German Bundestag, supported by the German Ministry of Economic Affairs and Energy via AiF within the framework of the program for the promotion of joint industrial research and development (IGF). Furthermore, the authors would like to thank Almatis GmbH for providing testing material as well as the other project partners involved for funding and support.

References

1 German, R.M., Bose, A.: Injection molding of metals and ceramics. Metal Powder Industries Federation, Princeton, 1997.

2 Reed, J.S.: Principles of ceramics processing. Wiley, New York, 1995.

3 Zhang, T., Blackburn, S., Bridgwater, J.: Debinding and sintering defects from particle orientation in ceramic injection molding, *J. Mater. Sci.*, **31**, 5891 – 5896, (1996).

4 Liu, L., Loh, N.H., Tay, B.Y., Tor, S.B., Murakoshi, Y., Maeda, R.: Effects of thermal debinding on surface roughness in micro powder injection molding, *Mater. Lett.*, **61**, 809 – 812, (2007).

5 Trunec, M., Cihlar, J.: Thermal debinding of injection molded ceramics, *J. Eur. Ceram. Soc.*, **17**, 203 – 209, (1997).

6 Trunec, M., Cihlar, J.: Thermal removal of multicomponent binder from ceramic injection mouldings, *J. Eur. Ceram. Soc.*, **22**, 2231 – 2241, (2002).

7 Xie, Z.P., Wang, L.L., Yang, X.F.: Study of water-debinding for ceramic parts by injection molding, *Mater. Sci. Forum*, 561 – 565, (2007).

8 Liu, D.-M., Tseng, W.J.: Influence of debinding rate, solid loading and binder formulation on the green microstructure and sintering behaviour of ceramic injection mouldings, *Ceram. Int.*, **24**, 471 – 481, (1998).

9 Shivashankar, T.S., German, R.M.: Effective length scale for predicting solvent-debinding times of components produced by powder injection molding, *J. Am. Ceram. Soc.*, **82**, 1146 – 1152, (1999).

10 Liu, D.-M., Tseng, W.J.: Binder removal from injection moulded zirconia ceramics, *Ceram. Int.*, **25**, 529 – 534, (1999).

11 Benzler, T.: Powder injection molding in microtechnology, dissertation in German, Freiburg, Universität Freiburg, Forschungszentrum Karlsruhe, 2001.

12 Franke, J.: Three-dimensional molded interconnect devices (3D-MID): Materials, manufacturing, assembly and application for injection molded circuit carriers, in German, Hanser Verlag, Munich, 2013.

13 Franke, J., Gausemeier, J., Goth, C., Dumitrescu, R.: MID-Study 2011-market and technology analysis. A study on behalf of the Forschungsvereinigung Räumliche Elektronische Baugruppen 3-D MID e. V., in German, Erlangen, 2011.

14 Komarov, S.V., Romankov, S.E.: Mechanical metallization of alumina substrate through shot impact treatment, *J. Eur. Ceram. Soc.*, **34**, 391 – 399, (2014).

15 Xin, C., Liu, W., Li, N., Yan, J., Shi, S.: Metallization of Al_2O_3 ceramic by magnetron sputtering Ti/Mo bilayer thin films for robust brazing to kovar alloy, *Ceram. Int.*, **42**, 9599 – 9604, (2016).

16 Hwang, H.R., Lee, R.Y.: The effects of metal coating on the diffusion bonding in Al_2O_3/Inconel 600 and the modulus of rupture strength of alumina, *J. Mater. Sci.*, **31**, 2429 – 2435, (1996).

17 Choa, B.-R., Leea, J.-J., Kang, S.-K.: Effect of composition change on sintering and metallizing of alumina ceramics, *J. Ceram. Process. Res.*, **10**, 121 – 123, (2009).

18 Zheng, Z., Zhang, Y., Yi, F., Chen, C., Song, X.: Surface metallization of alumina ceramics: effects of sintering time and substrate etching, *Ceram. Int.*, **40**, 12709 – 12715, (2014).

[19] Rong, C., Zhang, J., Liu, C., Yang, S.: Surface metallization of alumina ceramics by pulsed high energy density plasma process, *Appl. Surf. Sci.*, **200**, 104 – 110, (2002).

[20] Bulasara, V.K., Chandrashekar, O., Uppaluri, R.: Effect of surface roughness and mass transfer enhancement on the performance characteristics of nickel-hypophosphite electroless plating baths for metal-ceramic composite membrane fabrication, *Chem. Eng. Res. Des.*, **89**, 2485 – 2494, (2011).

[21] Forschungsvereinigung räumliche elektronische Baugruppen 3-D MID e. V.: 3D-MID technology: Spatial electronic assemblies: Manufacturing process, performance requirements, material properties, in German, Carl Hanser Verlag, Munich, 2004.

[22] Zhang, K.F., Lu, Z.: Surface features of polymer and ceramic microstructured parts manufactured by micro injection molding, Symposium on Design, Test, Integration and Packaging of MEMS/MOEMS, 212 – 217, 1999.

[23] Nickel, S.: Analysis of the ceramic injection molding process, dissertation in German, Erlangen-Tennenlohe: Lehrstuhl für Kunststofftechnik, 1998.

[24] Islam, A., Giannekas, N., Marhöfer, D.M., Tosello, G., Hansen, H.N.: Experimental investigation on shrinkage and surface replication of injection moulded ceramic parts, Proceedings of the 4th International Conference on Nanomanufacturing (nanoMan2014), 2014.

[25] Braun, T., Greiner, S., Franke, J., Drummer, D.: Additive plasma metallization of spatial ceramic injection molded components, 12th International Congress Molded Interconnect Devices, 62 – 67, 2016.